MESOSCALE GEOMETRIC MODELLING OF BIFURCATION IN 3D WOVEN T-BEAM PREFORMS

Louise P. Brown*, Shibo Yan, Xuesen Zeng and Andrew C. Long

Faculty of Engineering – Division of Materials, Mechanics & Structures, University of Nottingham, University Park, Nottingham, NG7 2RD, U.K.

*corresponding author: *louise.brown@nottingham.ac.uk*

ABSTRACT *Manipulation of the through-thickness yarn path enables 3D woven reinforcements to separate locally in the form of a bifurcation, creating net-shaped preforms for T- and I-beams. Preforming introduces fibre architecture deformation at the 3D woven bifurcation area. We report a geometric modelling approach to represent the realistic fibre architecture, as a preprocessing tool for finite element analyses. The study started with x-ray micro-computed tomography (µCT) of two 3D woven T-beams varying only by their weave patterns at the T-junction area. Supported by the µCT image analysis, a set of mathematical formulae were proposed to describe tow transformation, tow bending and tow flattening which were identified in the 3D woven T-beams. We then moved on to implement the automated modelling procedure in the open-source software TexGen. Using the weave pattern as input data, TexGen first simulates an as-woven flat T-piece. Next, TexGen applies geometric transformation and refinements to simulate the preforming process of T-beams. The paper highlights an efficient approach to model the complex woven bifurcation structure at mesoscale.*

INTRODUCTION

T- and I-beams are common structural elements in engineering applications. Carbon fibre composites T- and I-beams are regularly used as stiffeners in aircraft wing and fuselage structures. Currently aerospace-grade stiffeners are made from carbon fibre 2D reinforcement laminates. Net-shaped 3D woven T- and I- beam reinforcements reduce the manufacturing cost, and could potentially replace the 2D laminated stiffeners in aircraft, provided that 3D woven composites meet the mechanical performance requirement. The mechanical performance of fibre-reinforced composites is highly dependent on the meso-scale fibre architecture. It is essential to understand the relation between fibre architecture and performance in order to find optimum 3D woven T- and I beams for the intended application.

Investigations into 2D laminate T-beams revealed that laminar interface and resin-rich noodle area were the critical factors for the tensile strength [1, 2]. A number of studies were published on the performance of z-pin reinforced 2D laminate T-beams [3-6]. Although z-pin enhanced the inter-laminar strength, the insertion of z-pins caused fibre damage, compromising the in-plane performance[7]. Hao et. al. [8] investigated the impact performance of 3D woven T-beams. They stitched three pieces of 3D orthogonal woven fabric to form the web and flange, similar to the z-pinned 2D laminate process. Net-shaped T-beams can be produced from a specially developed weaving loom [9] or from a commercial Jacquard machine [10]. Up to now, there is little literature on characterization of net-shaped 3D woven T-beams.

We aim to develop a dedicated modelling wizard in TexGen to generate realistic 3D woven T-beam preforms. This study aligns along our established modelling approaches on 3D woven

reinforcement [11] and deformed 2D woven laminate [12]. TexGen will efficiently enable users to perform FE analyses based on the geometric model.

MATERIALS

The selected model materials were produced from a Jacquard machine. The net-shaped 3D woven T-pieces were flat from the weaving loom. They were then folded and compacted to form the T-beams in a mould with specified cavity thicknesses. The mould consisted of spacers, one flat plate and two L-shaped parts with fillets of 2 mm radius. The 3D woven fabrics used Hexcel IM7 12K carbon fibre tows as warp, weft and through-thickness binder tows in a proportion of 42:42:16. The web and flange regions of the T-beams were in 3D orthogonal weave style. The T-beams consisted of 8 layers of warp yarns and 9 layers of weft yarns in the web, and 4 layers of warp yarns and 5 layers of weft yarns in the flange. The mould resulted in a T-beam with web thickness 4 mm and flange thickness 2 mm. The overall fibre volume fraction was 45%. The directions of weft yarn, warp yarn and binder yarn are shown in Figure 1. There were two variations in weft yarn path at the noodle area. Variation I kept the same sequence of weft tows relative to each other, while Variation II had weft tows crossing over each other at the noodle area. The actual fibre architectures at the noodle area were visualised for Variation I and II in Figure 1.

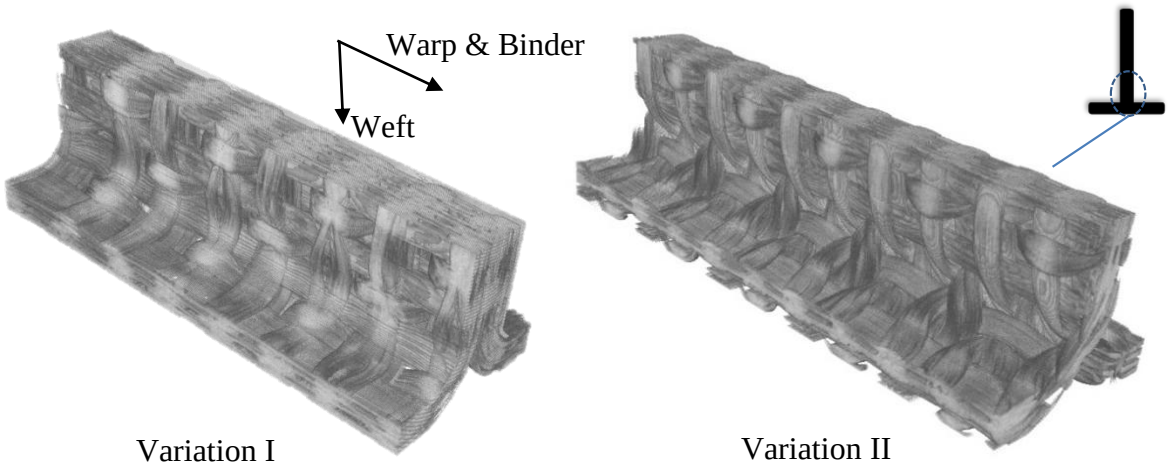

Figure 1. Two versions of net-shaped 3D woven T-beams: weft tows in Variation I are in the same position relative to each other while weft tows in Variation II cross over each other at the noodle area. The images are visualised via volume rendering from x-ray micro computed tomography.

IMAGE ANALSES

To characterize the intrinsic geometric features of the net-shaped T-beams, we used x-ray micro computed tomography (GE phoenix v|tome|x m, with a current of 240 μA and a voltage of 120kV). The scans achieved a resolution of 30 μm per pixel. The 3D images were processed and measured in ImageJ. We present three type of fibre architecture features, based on the μCT image analysis.

a) Warp yarn shift

The first distinctive deformation is the shift of warp yarn stack in the noodle region (Figure 2). The warp yarns within the same stack are aligned vertically with each other before folding the preform. Their relative positions are shifted afterwards. The warp yarn shift is inevitable due to the rigid body transformation in the noodle area. Each warp yarn has a different radius

to the fillet origin *O*. As illustrated in Figure 2, R_1^{weft}, R_2^{weft} and R_3^{weft} are the radii of centrelines for weft yarn 1, 2 and 3 respectively. As the radius of the inner surface of a T-piece is confined by the mould corner radius R_m, we can obtain:

$$\begin{aligned} R_1^{weft} &= R_m + \frac{H_{weft}}{2} \\ R_2^{weft} &= R_1^{weft} + D_{weft} \\ R_3^{weft} &= R_2^{weft} + D_{weft} \end{aligned} \qquad \text{(Eq. 1)}$$

Where H_{weft} is the weft yarn height; D_{weft} is the adjacent layer spacing of weft yarn. Assuming there is no yarn sliding, the shift angle S_θ(in radians) can be expressed as:

$$S_\theta = \frac{2(D_{warp} - d_o)}{R_1^Y + R_2^Y} - \frac{2(D_{warp} - d_o)}{R_2^Y + R_3^Y} \qquad \text{(Eq. 2)}$$

Where D_{warp} is warp yarn spacing within the same layer, and d_o the offset distance from the centre of nearest unbent weft yarn describing the position where the weft yarns start to fold; therefore $D_{warp} - d_o$ denotes the arc length in between bending onset position and bent yarn centre along the bend. $(R_1^{weft} + R_2^{weft})/2$ and $(R_2^{weft} + R_3^{weft})/2$ are the radii of centrelines for warp yarns on layer 1 and 2(R_n^{warp} where n equals 1 or 2).

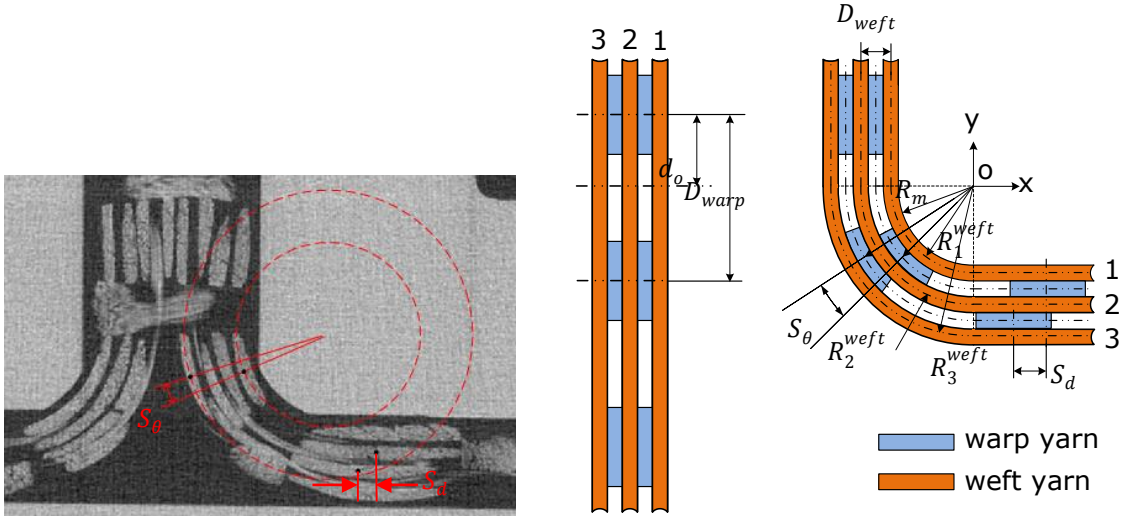

Figure 2.Left, measurement of warp yarn shift in the µCT images; Middle and right, schematic view of warp yarn shift due to rigid body transformation.

b) Warp yarn bent cross-section

Bent cross-sections of warp yarns were observed in the noodle region (Figure 2). The weft yarns comply with the fillet geometry of the mould surface. We approximate that the major axis of the bent cross-sections of warp yarns follow circular paths with different radii. The cross-section of one warp yarn is presented in Figure 3 prior to and after the deformation. According to the specified coordinate system, the original cross-section (the dashed line in Figure 3) can be defined parametrically as:

$$\begin{aligned} C(t)_x &= f(t) \quad 0 \le t \le 2\pi \\ C(t)_y &= q(t) \quad 0 \le t \le 2\pi \end{aligned} \qquad \text{(Eq.3)}$$

It is assumed that the bent shape is a result of a simple conformation of the major axis from the axis X to the arc in radius R_n^{Warp} (Eq. 1). The transformation is applied through

$$\Delta x = R_n^{warp} \sin\left(\frac{C(t)_x}{R_n^{warp}}\right) - C(t)_x$$
$$\Delta y = R_n^{warp}\left(1 - \cos\left(\frac{C(t)_x}{R_n^{warp}}\right)\right) \quad \text{(Eq.4)}$$

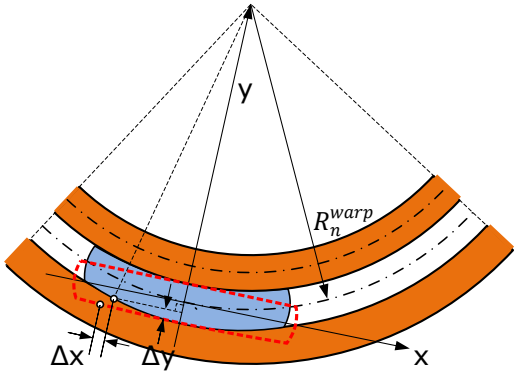

Figure 3. Coordinate definition for bent yarn cross-section.

c) Weft yarn flattening

In Figure 4, sectional view A-A shows the cross-sections of weft yarns at the noodle area, while B-B denotes cross-sections of weft yarns in the flat region. Table 1 listed the measurements of yarn width and yarn height at sections A-A and B-B. There was significant flattening in the weft yarns. Yarn flattening is caused by fibre repacking/migration due to bending high stiffness carbon fibre around a small radius.

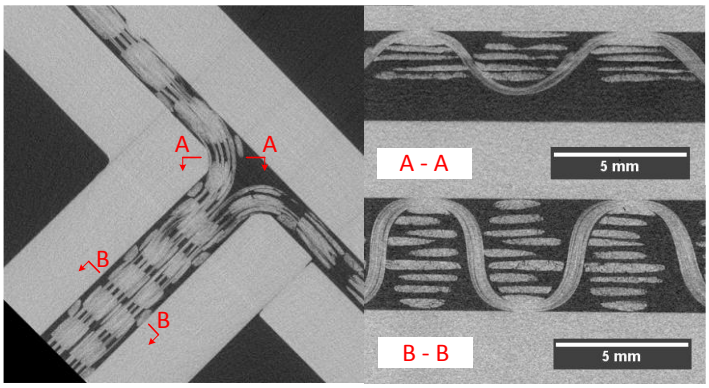

Figure 4. μCT images showing yarn flattening

Table 1 Cross-section parameters of weft yarn at A-A and B-B sections in Figure 4.

	Yarn height (mm) (±SD)	Yarn width (mm) (±SD)		Yarn height (mm) (±SD)	Yarn width (mm) (±SD)
A-A Layer 1	0.28(±0.01)	2.63(±0.08)	B-B Layer 1, 9	0.35(±0.03)	1.71(±0.07)
A-A Layer 2	0.29(±0.03)	3.01(±0.11)	B-B Layer 2 - 8	0.32(±0.03)	2.00(±0.13)
A-A Layer 5	0.29(±0.02)	3.57(±0.04)			

GEOMETRIC MODELLING AND IMPLEMENTATION

The T-pieces are modelled using TexGen open source software [13], firstly generating a model of the flat, as-woven textile, based on input from the weave pattern matrix. This

procedure has been automated and generates an idealised model to which refinements can be applied, based on observations from the µCT images, as described in the previous section. Transformations are then applied to the flat textile to create the bifurcation in the model.

a) Flat woven textile input

Creating a TexGen model from a weave pattern is carried out in two stages: firstly the weave pattern and layer information are read in from a text file and secondly the information is used to generate the cell structure used within TexGen for representing weave patterns.

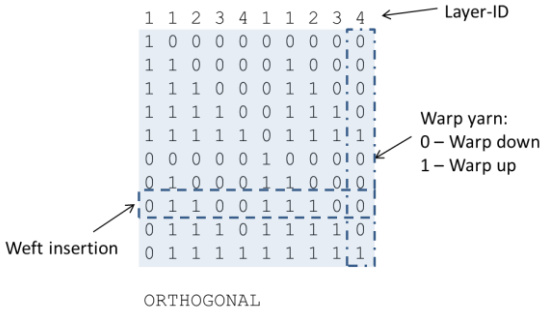

Figure 5. Weave pattern input file format

The weave pattern is shown in the shaded portion of Figure 5, in this case for a simple orthogonal weave. In order to reconstruct a textile model from the weave pattern extra information is supplied in the form of Layer-IDs as shown in Figure 5.

A Python script is used to read and process the input file from which the number of warp and weft yarns can be extracted and the position of binder yarns deduced. The TexGen CTextileOrthogonal class is used to create a textile which uses a three dimensional cell array to store the configuration of warp and weft yarns in the textile. The cell array is initialised by processing the weave pattern one row at a time utilising the Layer-ID information to delimit the binder and warp yarn stacks, illustrated by the dotted separators in Figure 6. For any stack of layers the weft yarn will be located above the first warp down entry and thus the weft position can be obtained.

For each binder/warp stack, j, the cell array is populated as illustrated in Figure 6 which shows the row for i = 2 as highlighted in Figure 5.

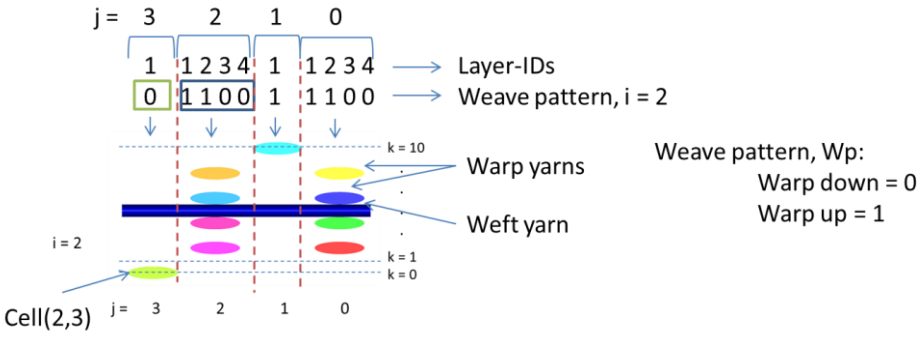

Figure 6. Creation of Cell Array entries from Weave Pattern Row

This produces a textile with warp yarns stacked but weft yarns spread out, one yarn for each cell row i. A subsequent process consolidates the textile, moving weft yarns into stacks between the binder yarns. The T-piece weave patterns vary slightly from standard orthogonal patterns; at the point where the textile divides into two layers one of the weft yarns crosses between two warp stacks, changing layer as it does so. In order to model this, a further yarn cell array was created to store the weft number so that, as the textile is consolidated, the

continuity of the weft yarns can be maintained. The as-woven textiles created are shown in Figure 7.

Figure 7. As-woven textile models. Left, Variation; Right, Variation II

b) Geometric Refinement

As can be seen in Figure 7 Right, the automation implemented in TexGen does not currently capture the interlacement of the weft yarns at the point where they cross over between layers. The order of weft insertions is known from the initial weave pattern and this, together with the yarn positions observed in slices taken through the µCT images in the transition area formed the basis for manual refinement of the TexGen model. Extra nodes were added at the mid-height of the transition area. Weft nodes on either side of these were also adjusted to reduce intersections with adjacent warp yarns. The refined textile is shown in Figure 8.

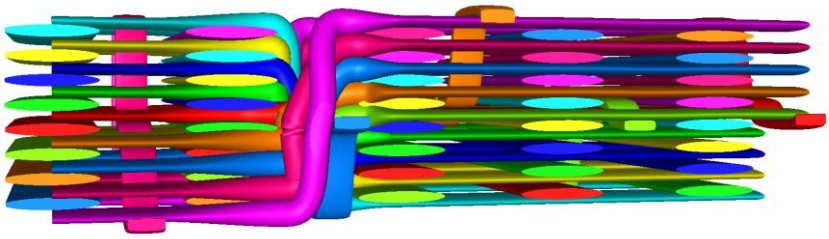

Figure 8 Variation II with yarns adjusted in the noodle area

c) T-piece transformation

The final stage of creating the T-piece model is to create the bifurcation. The tows are transformed in compliance to the mould tool surfaces *I* and *II* (Figure 9). The right-angle moulds *I* and *II* have a fillet with radius R_m, respective origins O' and O''. Rigid-body displacement and rotation is applied to the tows in the bifurcation region, according to their relative positions to surfaces I and II. To illustrate the transformation procedure, the following formulations are derived for a yarn that wraps around Surface *I*. One node on its yarn path has the local coordinates $[y', z']$ relative to origin O'.

The rotational angle, β, for yarn cross-section at $[y', z']$ in plane YZ is tangential to Surface I, given by

$$\beta = \begin{cases} \frac{y'}{z'} & for\ \frac{\pi}{2}z' \geq y' > 0 \\ \frac{\pi}{2} & for\ y' > \frac{\pi}{2}z' \end{cases}. \qquad \text{(Eq.5)}$$

The rotation is applicable to warp and binder yarns. No rotation is applied to weft yarns.

The translational displacements for Node $[y', z']$ are

$$\Delta y = \begin{cases} z'\sin\beta - y' & for\ \frac{\pi}{2}z' \geq y' > 0 \\ z' - y' & for\ y' > \frac{\pi}{2}z' \end{cases} \text{ and } \Delta z = \begin{cases} z'\cos\beta - z' & for\ \frac{\pi}{2}z' \geq y' > 0 \\ (\frac{\pi}{2}z' - y') - z' & for\ y' > \frac{\pi}{2}z' \end{cases}. \qquad \text{(Eq.6)}$$

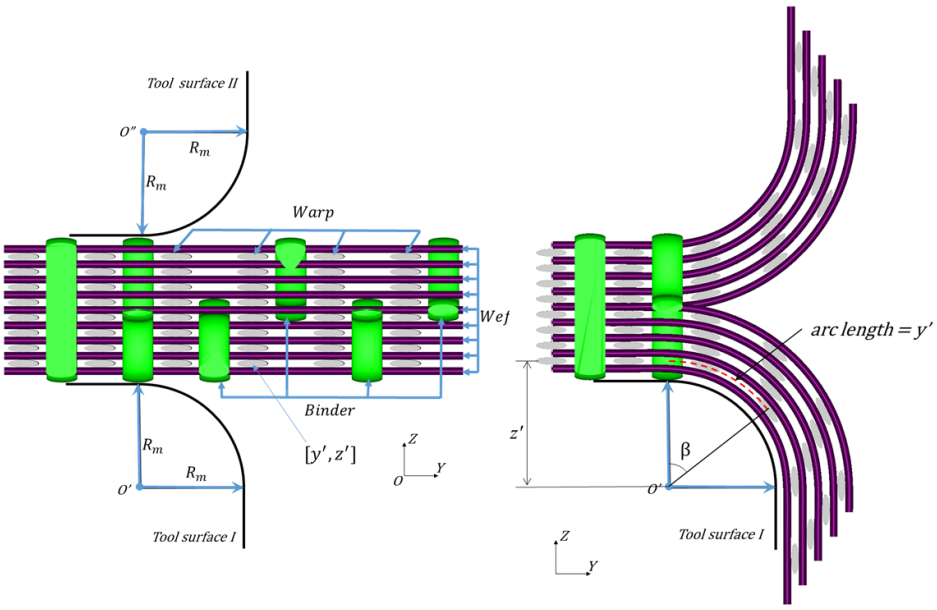

Figure 9. Configuration of bifurcation region

A Python script applies these transformations to the TexGen models as shown in Figure 10.

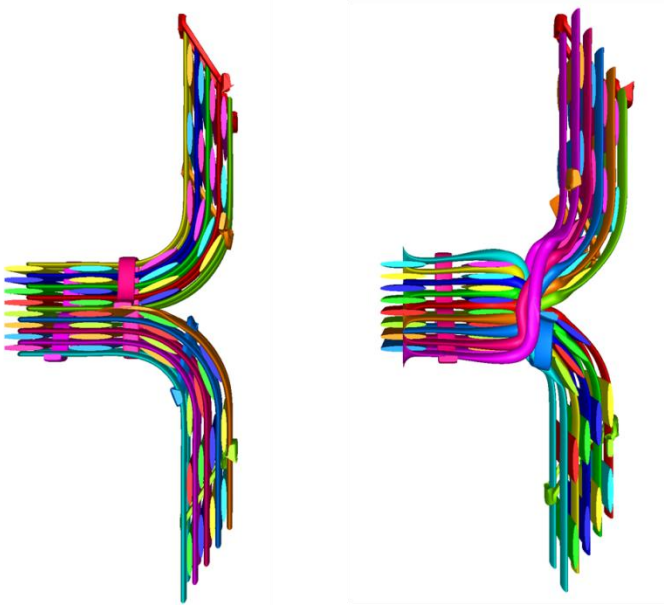

Figure 10Transformed T-piece models. Left, Variation I; Right, Variation II.

SUMMARY

Bifurcation is an important feature in net-shaped 3D woven reinforced T-/I- beams. To characterise the relationship between the fibre architecture and mechanical performance, the numerical simulation requires a realistic geometric model as input. In this study, based on the analyses of two net-shaped 3D woven T-beams, we approximated the geometry features analytically. The analyses informed the modelling implementation in TexGen, with input from the weave pattern providing an efficient method of creating the initial model. The TexGen models were broadly in agreement with the actual 3D woven T-pieces. Further refinements and validation will be pursued in the near future.

ACKNOWLEDGEMENTS

This work was supported by the Engineering and Physical Sciences Research Council - United Kingdom [grant number: EP/IO33513/1], through the EPSRC Centre for Innovative Manufacturing in Composites. The 3D woven fabrics were kindly supplied by SigmaTex. The x-ray µCT scans were conducted at Hounsfield Facility, University of Nottingham.

REFERENCES

[1] Hélénon F, Wisnom MR, Hallett SR, Trask RS. Numerical investigation into failure of laminated composite T-piece specimens under tensile loading. Composites Part A: Applied Science and Manufacturing. 2012;43(7):1017-27.

[2] Trask RS, Hallett SR, Helenon FMM, Wisnom MR. Influence of process induced defects on the failure of composite T-joint specimens. Composites Part A: Applied Science and Manufacturing. 2012;43(4):748-57.

[3] Koh TM, Feih S, Mouritz AP. Strengthening mechanics of thin and thick composite T-joints reinforced with z-pins. Composites Part A: Applied Science and Manufacturing. 2012;43(8):1308-17.

[4] Cartié DDR, Dell'Anno G, Poulin E, Partridge IK. 3D reinforcement of stiffener-to-skin T-joints by Z-pinning and tufting. Engineering Fracture Mechanics. 2006;73(16):2532-40.

[5] Park Y-B, Lee B-H, Kweon J-H, Choi J-H, Choi I-H. The strength of composite bonded T-joints transversely reinforced by carbon pins. Composite Structures. 2012;94(2):625-34.

[6] Toral Vazquez J, Castanié B, Barrau J-J, Swiergiel N. Multi-level analysis of low-cost Z-pinned composite joints: Part 2: Joint behaviour. Composites Part A: Applied Science and Manufacturing. 2011;42(12):2082-92.

[7] Mouritz AP. Review of z-pinned composite laminates. Composites Part A: Applied Science and Manufacturing. 2007;38(12):2383-97.

[8] Hao A, Sun B, Qiu Y, Gu B. Dynamic properties of 3-D orthogonal woven composite T-beam under transverse impact. Composites Part A: Applied Science and Manufacturing. 2008;39(7):1073-82.

[9] Soden JA, Weissenbach G, Hill BJ. The design and fabrication of 3D multi-layer woven T-section reinforcements. Composites Part A: Applied Science and Manufacturing. 1999;30(3):213-20.

[10] Amirul I. 3D woven structures and an overview of manufacturing techniques. 4th World Conference on 3D Fabrics and Their Applications. Aachen, Germany2012.

[11] Zeng XS, Brown LP, Endruweit A, Matveev M, Long AC. Geometrical modelling of 3D woven reinforcements for polymer composites: Prediction of fabric permeability and composite mechanical properties. Compos Part a-Appl S. 2014;56:150-60.

[12] Zeng XS, Endruweit A, Brown LP, Long AC. Numerical Prediction of In-plane Permeability for Multi-layer Woven Fabrics with Manufacture-induced Deformation. Composites Part A: Applied Science and Manufacturing. 2015 (doi: 10.1016/j.compositesa.2015.03.027).

[13] Long AC. and Brown LP, Modelling the geometry of textile reinforcements for composites: TexGen, in Composite reinforcements for optimum performance. P. Boisse, Editor 2011, Woodhead Publishing Ltd.